Proceedings of the 11th World Congress on Electrical Engineering and Computer Systems and Sciences (EECSS'25)
Paris, France - August, 2025
Paper No. EEE 142
DOI: 10.11159/eee25.142

Analysis of LLC Resonant DC-DC Converter with Non-Singular Fast Terminal Sliding Mode Control for Ev. Battery Charging

Mohammed Naji, Hur Jedi
Department of Electrical Engineering/ University of Kufa
Najaf, Iraq
mohammedh.halboos@student.uokufa.edu.iq; hur.jeddi@uokufa.edu.iq

Abstract **-** This paper introduces a non-singular fast terminal sliding mode (NFTSM) control approach for a novel full-bridge LLC unidirectional resonant a step-up DC-DC converter to improve the dynamic performance and stabilize the output voltage of the system. It is robust and suitable for charging high-power lithium-ion (Li-ion) batteries in Electric Vehicles (EVs). This converter is a new modification for a full-bridge LLC resonant DC-DC converter by connecting two converters in parallel with six MOSFET power. The power switches of the converter operate under soft-switching and Zero Current Switching (ZCS). Extended Description Function (EDF) is utilized to simplify large-signal model. A detailed analysis and theoretical approach are presented using linearization of second-order small-signal model. A closed-loop NFTSM control system is designed to provide regulated output voltage under a wide variation of input voltage. The measured results reveal that a high dynamic performance feature is obtained under multiple disturbance factors. The system operates at 100 kHz resonant frequency with various input voltage to achieve constant output voltage of 400 V.

Keywords**:** DC-DC converter, LLC resonant converter, Sliding mode control, PI controller, EV battery charger.

1. Introduction

Countries around the world have begun to improve the environment and address pollution. The major industrialized countries have started to make real plans for the near future to address one of the tools that cause pollution. EVs (Electric Vehicles) offer best alternative to internal combustion engines (ICE) vehicles [1]. This is what was witnessed in the Glasgow Agreement, which stipulates that ICE industries will cease at the beginning of the year 2035 in the European Union [2]. EVs are considered environmentally friendly and have begun to grow in all countries [3]. There are various types of EVs that require a battery charger [4]. DC-DC converter is a significant part of battery charging systems [5]-[7].

Previous researchers have studied LLC resonant DC-DC converter, which is considered one of the best types of converters due to achieving many features, such as soft-switching, and wide output voltage range, and high power [7]-[9]. This indicates the importance of having a special controller for the charger that protects the battery from unstable charging conditions or any disturbance to the system. In [10], the researchers used LLC resonant converter. The study focused on two control methods: Proportional-Integral-Derivative (PID) and Proportional-Integral-2 Derivative (PIDD2), including a comparison of two techniques. PIDD2 was employed as a preferred method for achieving high performance at various levels of input voltage. However, PIDD2 controller is not matched with high level of designed accuracy, especially when it comes with non-linearities as compare to sliding mode control technique. According to [11], a research group worked in design an LLC circuit with a high-frequency transformer using a solar energy as an input source and four MOSFET switches to operate as an inverter. The researchers used two control loops: the outer loop is used to control the output voltage, while the inner loop is employed to control the current of the converter. This method is called Constant Current Constant Voltage (CCCV). However, the proposed converter is not involved mathematical analysis and the design is complex. In [12], the research paper focused on the challenge of stabilizing the battery voltage under different operating conditions using the SMC method. However, it is not suitable for batteries operating at high voltages up to 400 DC.

The main objectives of this study are to present an LLC resonant DC-DC converter with the capability to operate at high power. Moreover, this study also presents a NFTSM control system with frequency mode control, including a battery charger that can achieve high dynamic response of the output voltage within a wide range of input voltages. The theoretical analysis and steady-state waveforms are analysed in details. The converter is operated at resonant switching frequency 100 kHz and fixed duty ratio. The simulation results show the demonstration of theoretical analysis of the converter at 7.2 kW. These features make the introduced converter advantageous in applications that require a high-power operation, such as Ev. charging systems and solar cell applications.

2. Analysis for the Proposed DC-DC Topology

Fig. 1 shows the proposed LLC resonant DC-DC converter. It consists of a power switching network, a resonant tank, a transformer, and an output rectifier filter circuit. The power switches S_1, S_2...S_6 with their parasitic capacitance C_{ds1}, C_{ds2}, ... C_{ds6} and parasitic anti-parallel diodes D_{ds1}, D_{ds2}, ...D_{ds6} forms the switching network of the proposed topology. The resonant tanks comprise of two resonant inductors (L_{r1}, L_{r2}), two magnetizing inductors (L_{m1}, L_{m2}), and two resonant capacitors (C_{r1}, C_{r2}). High-performance transformers Tr_1 and Tr_2 have the same characteristics with turns ratio $n_1 = n_2$. The rectifier circuit involves diodes as rectifying elements D_1, D_2, D_3 and D_4 for the first converter with output-filter capacitor C_{O1}, while D_5, D_6, D_7 and D_8 for the second converter with output-filter capacitor C_{O2}. The supply voltage V_I is first stage's output voltage of the AC/DC converter. The output voltage of the proposed topology is notated as V_O. The output current I_O provides the required current to the battery. To simplify the analysis, it is considered that both the transformers have the same turns-ratio $n = n_1 = n_2$ and the two magnetizing inductances are equal $L_{m1} = L_{m2}$. The power MOSFETs of the introduced converter are identical, including parasitic capacitances $C_{ds1} = C_{ds2}...C_{ds6}$.

2.1. Proposed LLC Resonant DC-DC Converter

In this paper, only one converter will be analysed and studied because the two converters have same characteristics. A full-bridge inverter is utilized to converter the DC input voltage to high-frequency square AC output voltage waveform. Then, the energy moves from the primary sides to the secondary sides of the transformers, while the magnetizing inductors L_{m1} and L_{m2} are clamped to nV_O. The resonance phenomenon occurs between L_r and C_r at resonant frequency f_o is

$$f_o = \frac{1}{2\pi\sqrt{L_r C_r}}. \tag{1}$$

The resonance can also occur among L_r, L_m, and C_r. Thus, the second resonance frequency can be expressed as

$$f_m = \frac{1}{2\pi\sqrt{(L_r + L_m)C_r}}. \tag{2}$$

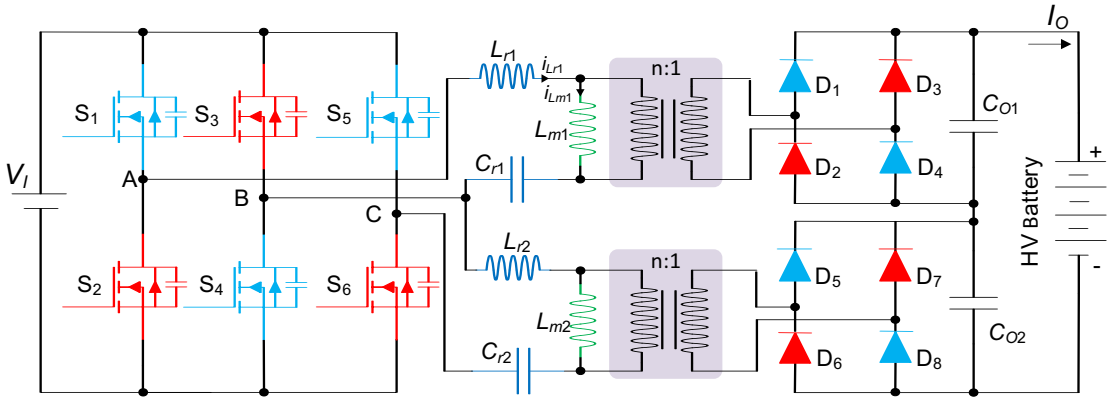

Fig. 1: Proposed LLC resonant DC-DC topology.

To obtain wide output voltage range of the proposed LLC resonant converter, pulse frequency modulation (PFM) is utilized to reduce or increase the switching frequency f_s. Since the proposed topology operates as step-up voltage converter, the range of switching frequency is $f_m < f_s < f_o$. The idealized waveforms of the proposed topology are depicted in Fig. 2. Since the proposed DC-DC topology has two symmetrical resonant tanks and transforms, the essential equations of the proposed circuit are derived according to the equivalent circuit model with one resonant tank. Thus, the normalized gain M is expressed as

$$M = \frac{8}{\pi^2}\frac{\omega_n^2(m-1)}{\sqrt{(m\omega_n^2-1)^2 + Q^2\omega_n^2(m-1)^2(\omega_n^2-1)^2}}. \tag{3}$$

Hence, the quality factor Q, which is the relation between the characteristic impedance and the resistance of the load, is

$$Q = \frac{\sqrt{L_r/C_r}}{R_e}, \tag{4}$$

and the relationship between the angular switching frequency ω_s and angular resonant frequency ω_o is

$$\omega_n = \frac{\omega_s}{\omega_o}. \tag{5}$$

The ratio of total equivalent magnetizes to the resonant inductor is

$$m = \frac{L_m}{L_r}. \tag{6}$$

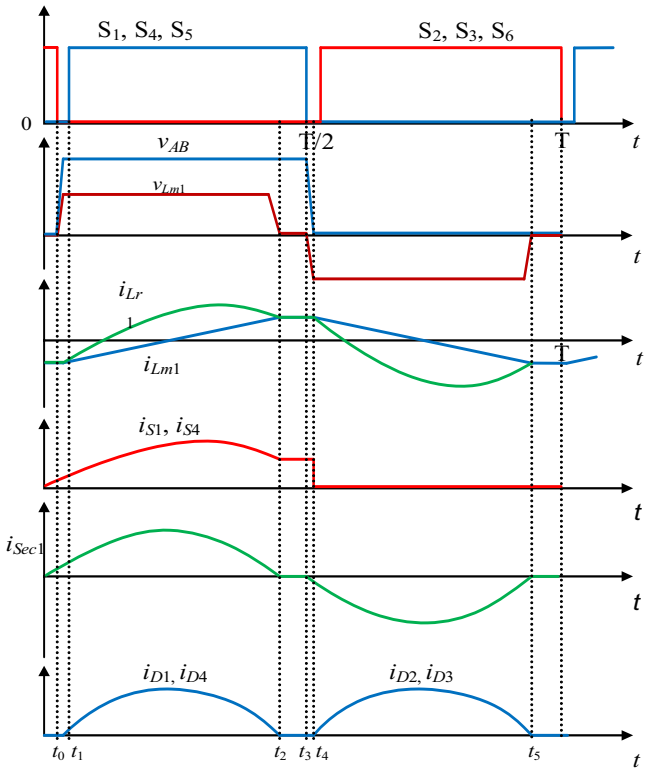

Fig. 2: The idealized waveforms of the proposed DC-DC converter.

From Eq. (3), the voltage gain of the introduced LLC resonant converter is illustrated in Fig. 3 at different values of Q. For light load conditions operate, the value of Q is small, while the heavy load indicates high value of Q. Moreover, it can be seen that all curves have unity gains and cross at the resonant frequency point at $\omega_n = 1$ or $\omega_s = \omega_o$. The purpose of defining two regions is to maintain an inductive operation across the entire load current range and avoid the capacitive region operation. This requirement stems from the fact that ZVS (Zero-voltage switching) technique can only be realized in the inductive region. The components of the proposed system are designed and calculated based on Eqs. (1) - (6). Furthermore, the values of Q and m are chosen with more than one attempt applied of the Eq. (3) to identify the optimal design values. Table. 1 shows the normalized design parameters of the proposed converter.

2.2. Time-Varying Parameters in Nonlinear System

Based upon the proposed circuit shown in Fig.1, the time-varying non-linear equations and the Kirchhoff law (KCL) is

$$X = \left[X_a\ X_b\ X_c\ X_d\right] = \left[i_{Lr}\ i_{Lm}\ v_{cr}\ v_o\right] \tag{7}$$

$$v_{AB} = u \tag{8}$$

$$y = X_d, \tag{9}$$

where the currents i_{Lr}, i_{Lm}, and the voltages v_{Cr}, v_o are the state variables, while v_{AB} is the input voltage of the converter. Assuming all components of the proposed circuit are ideal. Its behaviour can be defined as the following state-space non-linear Eqs. (10) – (12)

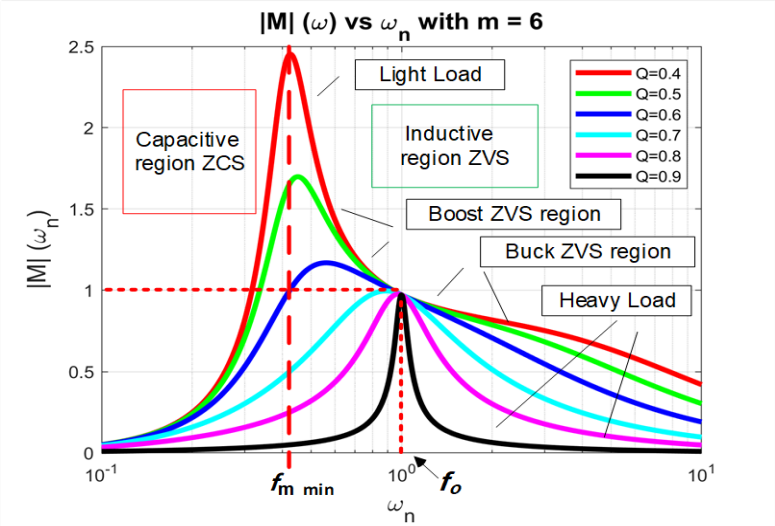

Fig. 3: Characteristic of LLC resonant converter.

$$i_{Lr} = C_r \frac{dv_{cr}}{dt} \tag{10}$$

$$\frac{di_{L_r}}{dt} = \frac{di_{L_m}}{dt}\left(-\frac{L_m}{L_r}\right) + \frac{1}{L_r}\left(v_{AB} - v_{C_r}\right) \tag{11}$$

$$\frac{di_{L_m}}{dt} = \frac{nv_o}{L_m} sgn\left(i_{L_r} - i_{L_m}\right). \tag{12}$$

Sub Eq. (12) in Eq. (11) and simplify the equation. The variable quantities are expressed as

$$\dot{X}_a = \left[\frac{1}{L_m}\left|X_a - X_b\right| * X_d * n\right]\left(\frac{-L_m}{L_r}\right) + \frac{1}{L_r}\left(u - X_c\right) \tag{13}$$

$$\dot{X}_b = \frac{1}{L_m}\left|X_a - X_b\right| * X_d * n \tag{14}$$

$$\dot{X}_c = \frac{i_{L_r}}{c_r} \tag{15}$$

$$\dot{X}_d = \left[\frac{1}{C_o}\left(n * \left|X_a - X_b\right| - \frac{X_d}{R_L}\right)\right]. \tag{16}$$

2.3. Seventh-Order Large Signal Model

In the previous subsection, FHA (First Harmonic Approximation) model was utilized to represent system's behaviour under large-signal model. The state quantity of Eqs. (13) – (16) can be converted as a combination of sine and cosine functions with frequencies associated to f_s. Some non-linear parts can be linearized by Extended Description Function (EDF) method. Then, the model of seventh-order large signal, which based on the EDF method, can be constituted by [13][14]

$$i_{L_r} = I_{L_{rs}} * \sin\left(\omega_s t\right) + I_{L_{rc}} * \cos\left(\omega_s t\right) \tag{17}$$

$$i_{L_m} = I_{L_{ms}} * \sin\left(\omega_s t\right) + I_{L_{mc}} * \cos\left(\omega_s t\right) \tag{18}$$

$$v_{c_r} = V_{c_{rs}} * \sin\left(\omega_s t\right) + V_{c_{rc}} * \cos\left(\omega_s t\right) \tag{19}$$

$$v_{AB} = \frac{4 * V_o}{\pi} * \sin\left(\pi d\right) * \sin\left(\omega_s t\right), \tag{20}$$

where the symbols 's' and 'c' are assigned to sine and cosine functions, and ω_s is the angular switching frequency.

2.4. Simplified Second-Order Small Signal Equivalent Model

The equivalent model of the seventh-order large-signal is complex because it has some nonlinear terms that are generated by the product of two or three parts of variables. To simplify the design of control system, the seventh-order model can be linearized and decreased at the resonant point to attain the 2'nd order linear small-signal model [9]. Then, the transfer function of the system can be found and can be expressed as [15][16]

$$H_{vf}(s) = \frac{n_f}{d_1 s^2 + d_2 s + 1}, \tag{21}$$

where

$$n_f = \frac{\delta v_o}{\delta f_s} = -\frac{8 L_m V_I}{L_r f_r \pi n} \tag{22}$$

$$d_1 = \frac{\pi^2}{4}\frac{C_o L_r}{n^2} \tag{23}$$

$$d_2 = \frac{\pi^2}{4}\frac{L_r}{R_L n^2}. \tag{24}$$

3. NFTSM Controller Design for Proposed Converter

The aim of controller is to make the resonant LLC DC-DC converter reliable and handle with the disturbances from the input side. The frequency f_s, which is described as the input variable, is an essential parameter. Hence, the state variable x_1 is selected as the error signal between the actual output voltage v_O and the reference voltage V_{REF}, which is a constant value.

$$x_1 = v_o - V_{REF} \tag{25}$$

$$x_2 = \dot{x}_1 \tag{26}$$

where x_2 is the rate of change of the error signal over time. Eq. (28) and Eq. (29) express the relationship between the actual output voltage v_O and the small signal disturbance of the output voltage $\hat{v}_o$, while the relationship between the small signal disturbance of the switching frequency $\hat{f}_s$ and the switching frequency f_s are

$$v_o = V_O + v_o \tag{27}$$

$$f_s = F_s + f_s \tag{28}$$

where F_s indicates the frequency at the resonant point, and the output voltage V_O is chosen at the resonant point.
By using the inverse Laplace transform of Eq. (21) and utilizing Eq. (28), the relationship in time domain of v_o and f_s is

$$\ddot{v}_o = \frac{\left[V_O + n_f\left(f_s - F_s\right) - d_2 \dot{v}_o - v_o\right]}{d_1} \tag{29}$$

Based on Eqs. (25) – (29), the state variables are

$$\dot{x}_1 = \dot{v}_o \tag{30}$$

$$\dot{x}_2 = \frac{V_O + n_f\left(f_s - F_s\right) - d_2 \dot{v}_o - v_o}{d_1}. \tag{31}$$

The NFTSM surface of the proposed LLC resonant DC-DC converter is designed according the general formal Eq. (32)

$$s = k\, x_1 + c\, x_2 + \beta\, x_2^{\frac{\lambda}{\alpha}} \tag{32}$$

$$c = \begin{cases} \Psi & |x_1| \geq 1 \\ \Psi |x_1|^{\delta} & |x_1| < 1 \end{cases}$$

k, β, and Ψ are constants greater than zero, $\delta >= 1$. While the parameters λ and α are odd numbers, $\lambda/\alpha > 1$. It is clear that NFTSM system consists the characteristics of NTSM and LSM (Linear Sliding Mode). The state of the system converges

exponentially when the actual output voltage deviates far from the reference voltage $|x_1| \geq 1$ to improve the dynamic characteristic of the system. By utilizing the exponential approach, the designed NFTSM controller can be expressed as

$$u = \frac{d_1}{n_f}\left[\frac{-k}{c+\frac{\beta\lambda}{\alpha}x_2^{\frac{\lambda}{\alpha}-1}}x_2 + \frac{d_2}{d_1}x_2 + \frac{\left(V_{REF}+x_1-V_o\right)}{d_1} - \sigma\, sgn\left(s\right) - \gamma\, s\right] + F_s \tag{33}$$

where $\sigma, \gamma > 0$. Fig. 4 shows block diagram of NFTSM controller closed-loop of the proposed LLC resonant power converter.

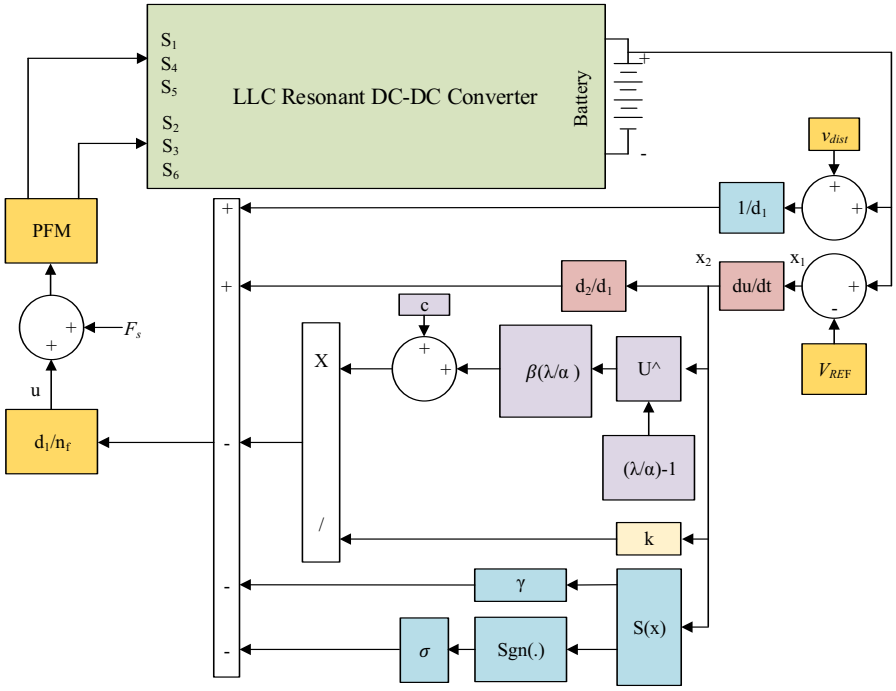

Fig. 4: Block diagram for the closed-loop NFTSM of the proposed LLC resonant DC-DC converter.

The block diagram describes the NFTSM controller scheme with the proposed converter. The controller measures the output voltage by a voltage sensor then compares it with the required reference voltage. The controller generates required signal and combined it with the working frequency. Then, the signal is sent to the PFM block, which provides pulses to the power MOSFET switches (S_1, S_2… S_6).

Table 1: Parameters design of proposed LLC resonate DC-DC converter.

	Symbol	Description	Value	Unit
Proposed Converter	V_I	Input Voltage	200	V
	V_O	Output Voltage	400	V
	P_O	Output Power	7.2	kW
	L_{r1}, L_{r2}	Resonant Inductance	8.49	µH
	C_{r1}, C_{r2}	Resonant Capacitance	0.29	µF
	L_{m1}, L_{m2}	Magnetizing Inductance	16.98	µH
	n_1, n_2	Transformer Turns Ratio	0.5	
	f_o	Resonant Frequency	100	kHz
PI Controller	K_p	Proportional Gain	0.0034	-
	K_I	Integral Gain	72.039	-
NFTSM	K	Linear Coefficient	5	-
	C	Linear Coefficient	1	-
	β	Non-Linear Coefficient	150	-

4. Results and Discussion

In this section, the proposed topology LLC resonant DC-DC converter and NFTSM control method are established in Simulink-MatLab, using the parameters listed in Table I. In order to verify the theoretical analysis, the characteristics of NFTSM control system and the performance of battery charger, a PI control method (K_P and K_I) is utilized as a contrast. It is worth noticing that the NFTSM control parameters have been optimized based on small-signal analysis of EDF method.

Fig. 5 shows the waveforms of the output voltage across the load under reference voltage 400 V and 200 V input voltage. For comparison between NFTSM controller and PI controller, the output voltage accurately tracks the reference voltage and reach the set reference voltage. The NFTSM control unit is characterized by high resistance to disturbance. This control system can directly switch to the normal work state and transmit the output voltage without any change. It can be seen that the response of output voltage under NFTSM control method when the input voltage suddenly changes as illustrated in Fig. 6. When the required reference voltage changes throughout the system operation, the output voltage follows the reference voltage as shown in Fig. 7.

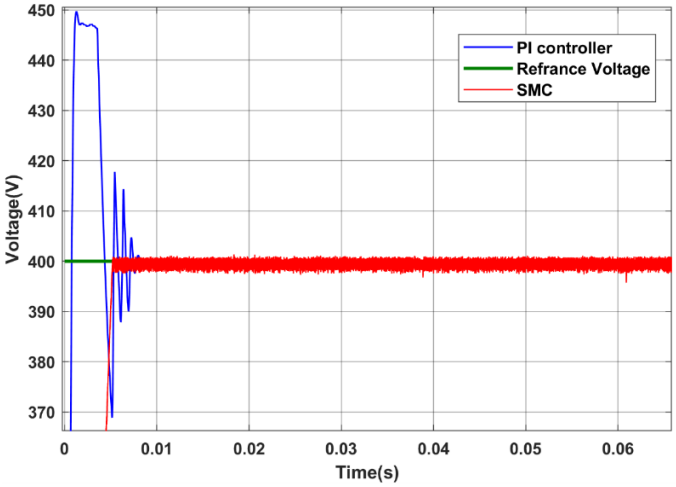

Fig. 5: The output voltage waveform at input 200 V.

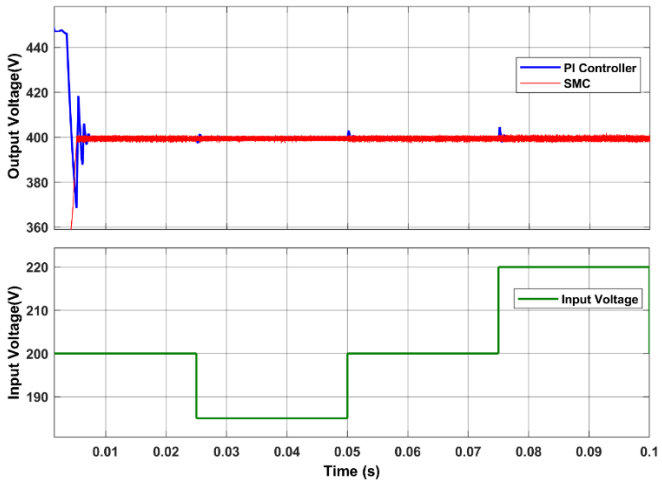

Fig.6: The output voltage waveform at input range (180-220) V.

The results indicate that the overshoot of PI controller and NFTSM controller are 13% and less that 1%, respectively. In addition, the settling time of PI controller is 1.9 ms, while the settling time of NFTSM is 1.9 ms.

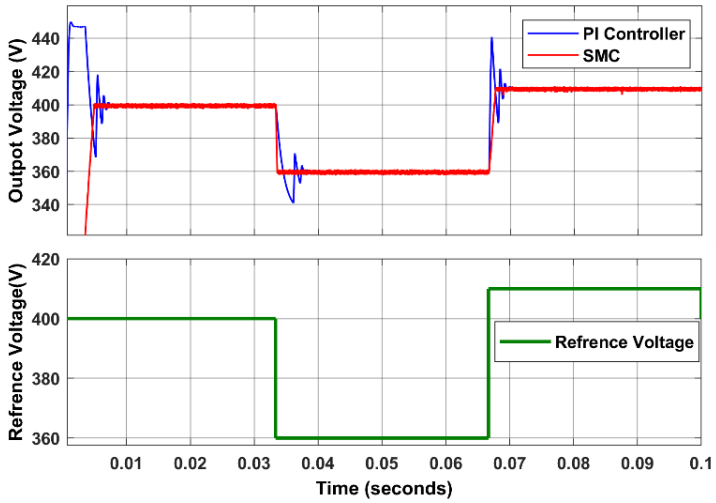

Fig.7: Output voltage with reference voltage range (360-410) V.

The comparison results between the two types indicate that NFTSM offers high performance to the traditional PI controller. This leads to significantly improve the operation of the LLC resonant DC-DC converter. Furthermore, the NFTSM controller is more stable, but the drawback of the phenomenon is chattering. The PI controller is slow and has an overshoot that takes time to reach a stable state. Since EVs' battery packs are sensitive to voltage surges, it is required to provide safety, stable and accurate charging system throughout the charging period of the Li-ion battery.

5. Conclusion

This work has been introduced a NFTSM control topology of a novel LLC resonant DC-DC isolated converter that achieves high performance as a reliable EV charger. All switches work on the principle of ZVS and ZCS techniques. The study aimed to analyse the proposed converter in steady-state using FHA. The research utilized two control methods NFTSM and PI controller. The NFTSM controller provides highly efficient converter that works with a variation of input voltages and supplies a stable output voltage. The proposed topology can be used as a reliable power supply for battery charging in EVs due to its advantages that realizes high power and thereby reduces the charging time.

References

[1] N. Tilly, T. Yigitcanlar, K. Degirmenci, and A. Paz, "How sustainable is electric vehicle adoption? insights from a prisma review", *Sustainable Cities and Society*, vol. 117, no. 1, pp. 1-22, 2024.

[2] S. Grzesiak and A. Sulich, "Car engines comparative analysis: sustainable approach," *Energies*, vol. 15, no. 14, 2022.

[3] M. Shahed and A. Rashid, "Battery charging technologies and standards for electric vehicles: a state-of-the-art review, challenges, and future research prospects," *Energy Reports*, vol. 11, pp. 5978–5998, 2024.

[4] P. Dini, S. Saponara, and A. Colicelli, "Overview on battery charging systems for electric vehicles," *Electron*., vol. 12, no. 20, 2023.

[5] A. Vazani, H. Mirshekali, N. Mijatovic, V. Ghaffari, R. Dashti, H. Shaker, M. Mardani, and T. Dragičević, "Composite nonlinear feedback control of a DC-DC boost converter under input voltage and load variation," *Int. jour. of Ele. Power and Energy Sys*., vol. 155, pp. 1–13, 2024.

[6] J. Šimko, M. Praženica, R. Koňarik, and P. Koteš, "The analysis , modeling , and control of the forward DC / DC the analysis , modeling , and control of the forward DC / DC converter for the electric vehicle converter for the electric vehicle," *Transp. Res. Procedia*, vol. 74, pp. 831–837, 2023.

[7] O. Ghazal, M. Marei, and A. Mohamad, "Small-signal modeling comparison of dual active bridge converter," *e-prime - Adv. Electr. Eng. Electron. Energy*, vol. 8, pp. 1-9, 2024.

[8] H. Xu, T. Hu, C. Yu, Z. Wu, X. Yin, and B. Lu, "Research on full-bridge LLC resonant circuit under compound control of input compensation," 5*th Asia Energy Electr. Eng. Symp*., Chengdu, China, 2023, pp. 863–868.

[9] A. Memon, M. Gulzar, N. Bashir, S. Habib, A. Shakoor, and F. Ehsan, "Optimal control method for LLC resonant convertor of EV battery chargers," in *Proc Int. Conf. Renew. Energy Res. Appl.*, Nagasaki, Japan, 2024, pp. 992–997.

[10] K. Sathya and K. Guruswamy, "Analysis of LLC resonant converter performance with PIDD2 controller for electric vehicle application," *Indones. J. Electr. Eng. Comput. Sci*., vol. 37, no. 2, pp. 749–757, 2025.

[11] K. Anjali, P. Mohan, M. Unnikrishnan and Lakshmipriya, "PV fed off-board e-bike battery charger using LLC resonant converter," in *Proc Int. Conf. Adv. Power, Commun. Intell. Syst*., Kannur, India, 2024, pp. 1–6.

[12] A. Taheri and N. Asgari, "Sliding mode control of LLC resonant DC-DC converter for wide output voltage Range in battery charging applications," *Int. J. Ind. Electron. Control Optim*., vol. 2, no. 2, pp. 127–136, 2019.

[13] J. Shahsevani and R. Beiranvand, "Application-oriented review of the LLC-based resonant converters," *IEEE Access*, vol. 12, no. April, pp. 52687–52726, 2024.

[14] M. Saadati, A. Ghayebloo, and A. Taheri, "A novel analog controller design scheme for LLC resonant converter used in battery charging application," *IET Power Electron*., vol. 15, no. 9, pp. 802–814, 2022.

[15] J. Lu, "Integral global fast terminal sliding mode control for LLC converters," *J. Phys. Conf. Ser*., vol. 2797, no. 1, 2024.

[16] X. Niu, X. Hu, and X. Li, "Full-bridge LLC resonant converter with super-twisting non-singular fast terminal sliding mode control," in *Proc. IEEE 7th Int. Electr. Energy Conf.*, Harbin, China, 2024, pp. 2138–2143.